El Cezeri
Journal of Science and Engineering
ISSN: 2148-3736

Research Article

# Evaluation and Improvement of Power System Security with the Application of Machine Learning

**Peruthambi Venkatesh[1a], Nagalamadaka Visali[2b]**
[1] Research scholar, Jawaharlal Nehru Technological University Anantapur, Ananthapuramu-515002, Andhra Pradesh, India.
[2] Professor, Department of Electrical Engineering, JNTUA College of Engineering, Constituent College of Jawaharlal Nehru Technological University Anantapur, Ananthapuramu-515002, Andhra Pradesh, India
venkateshp.engg@gmail.com

DOI : 10.31202/ecjse.1316748
Received: 19.06.2023 Accepted: 15.01.2024
**How to cite this article:**
Venkatesh, P., Visali, N., " Evaluation and Improvement of Power System Security with the Application of Machine Learning", El-Cezeri Journal of Science and Engineering, Vol: 11, Iss:1, (2024), pp.(48-57).
ORCID: [a]0000-0003-3124-5396; [b] b0000-0001-5194-5854.

**Abstract :** Numerous renewable and nonrenewable energy sources have been integrated into the grid by utilities to keep up with rising demand. Problems with the generator, transmission lines, and distribution networks are exacerbated by sudden load changes. The representation of load plays a crucial role in system prediction, and based on research results, ZIP load models incorporating contingency criteria have proven successful in predicting future load behavior. To forecast the severity of line losses and predict system reactions, an Artificial Neural Network (ANN) is trained, while the NR technique utilizes the High Bridge Line Stability Ranking Index (HLSRI) to predict contingency ranking during a single-line failure. Stability and cost analysis, with and without the Unified Power Flow Controller (UPFC) and Interline Power Flow Controller (IPFC), has been conducted using a mathematical model. Machine learning (ML) is employed to rapidly identify the transmission line most affected by an emergency. The J48 method is used for data clustering to determine the placement of compensatory devices. Additionally, the Particle Swarm Optimization (PSO) method establishes an appropriate goal function to reduce fuel consumption and increase output. The research emphasizes the critical role of power outages and fluctuating loads. The power grid's status is determined through power system security analysis. In this context, a broken transmission line or a change in load has the potential to harm the electrical system.

**Keywords :** High bride Line Stability Ranking Index (HLSRI), Interline power flow controller (IPFC), Machine Learning (ML), Unified Power Flow Controller (UPFC).

## 1 Introduction

The expansion of renewable energy sourcMultilayered electricity is required for modern life, emphasizing the essentiality of electrical grid reliability. The security of the power system is crucial to ensure a dependable power supply to clients, without compromising the safety of the power grid, user well-being, or profitability. Unfortunately, this intricate power system is susceptible to various challenges such as transmission line failure, generator malfunction, load demand spikes, and transformer destruction. The significance of electricity system safety cannot be overstated, as power system oscillations contribute to the escalation of blackouts. The ramifications are profound, leading to business bankruptcies and significant disruptions in the lives of average individuals. Identifying the underlying causes of blackouts is imperative, necessitating the development of a deliberate plan to prevent their propagation to other lines. A contingency analysis, encompassing both operation and maintenance, serves as a rapid assessment tool for evaluating the system's stability after an outage or abnormal state. The responsibility for addressing any deviations from normal functioning that may arise when a problematic component is removed from the system lies with the backup plan. A substantial disruption in line flow can trigger overloads in other lines, setting off a domino effect on adjacent strings. Prompt action by the regulator is imperative when a line outage results in a surge in demand. Power system operators and planners must consistently consider all potential consequences. The technique of contingency screening employs a diverse array of static and time-dependent approaches to categorize prospective outcomes, ensuring a comprehensive evaluation of possible scenarios [1] [2].

To meet increasing demand, several renewable and non-renewable energy sources have been incorporated into the electricity system. The challenges posed by abrupt fluctuations in load exacerbate concerns related to generators, transmission lines, and distribution networks. The accuracy of system predictions relies heavily on load modeling. This study demonstrates that ZIP load models, coupled with contingency criteria, can effectively forecast load behaviour. In the event of a single line outage, the

NR technique employs the HLSRI to anticipate contingency rankings. An ANN is then trained to anticipate the severity of the outage and the system's response. A mathematical model is employed to compare stability and costs with and without the UPFC and IPFC. Machine learning swiftly identifies which transmission line is most vulnerable during emergencies by utilizing the J48 method to cluster data for compensatory device development. The PSO algorithm optimizes production capacity to minimize fuel expenditures. The electrical system faces potential damage from both transmission line failures and load variations. This study highlights transmission line breakdowns and load changes as primary concerns. A power system security study is conducted to assess its current status.

## 2 Problem Formulation

### 2.1 Load Modeling

Most emergencies are caused by changes in load and load modeling aids in the analysis of diverse loads. Mathematically, load modeling depicts the power-voltage relationship at a load bus. Power system research is impacted by it [3]. This study encompasses two types of load models.

### 2.2 Constant Load Model

In the steady-state load model, Equations 1 and 2 illustrate the active and reactive power, respectively.

$$P_i = \sum_{j=1}^{n} V_i Y_{ij} V_j \cos\left(\theta_{ij} + \delta_j - \delta_i\right) \tag{1}$$

$$Q_i = -\sum_{j=1}^{n} V_i Y_{ij} V_j \sin\left(\theta_{ij} + \delta_j - \delta_i\right) \tag{2}$$

Active/reactive power is diagonal and half-diagonal is designed for $P_i$and $Q_i$.

### 2.3 Polynomial Load Model or ZIP Load Model

The term "ZIP" stands for "polynomial load model," with Z, I, and P representing constant impedance, current, and power, respectively. The driving forces of the model are encapsulated in Equations 3 and 4. At Bus-i:

$$P_i = \left[\sum_{j=1}^{n} V_i Y_{ij} V_j \cos\left(\delta_{ij} + \theta_j - \theta_i\right)\right]\left[P_1 V_i^2 + P_2 V_i + P_3\right] \tag{3}$$

$$Q_i = \left[-\sum_{j=1}^{n} V_i Y_{ij} V_j \sin\left(\delta_{ij} + \theta_j - \theta_i\right)\right]\left[P_1 V_i^2 + P_2 V_i + P_3\right] \tag{4}$$

At Bus-j:

$$P_j = \left[\sum_{i=1}^{n} V_j Y_{ji} V_i \cos\left(\delta_{ji} + \theta_i - \theta_j\right)\right]\left[P_1 V_j^2 + P_2 V_j + P_3\right] \tag{5}$$

$$Q_j = \left[-\sum_{i=1}^{n} V_j Y_{ji} V_i \sin\left(\delta_{ji} + \theta_i - \theta_j\right)\right]\left[P_1 V_j^2 + P_2 V_j + P_3\right] \tag{6}$$

where active and reactive power values at buses i and j are $P_i$, $P_j$ and $Q_i$, $Q_j$; $V_i$, $V_j$ are nodal voltages at bus i, j; $\delta_{ij}$ is the voltage angle; $Y_j i$ is the admittance; The parameters for the ZIP load are denoted by the letters $P_1$, $P_2$, and $P_3$.

Active and reactive power in Bus-i and Bus-j are distributed both diagonally and off-diagonally. The solution to load models is achieved through the Newton-Raphson power flow method, which yields accurate quadratic convergence results. The creation of diagonal and off-diagonal elements in Equation 7 results in a Jacobian matrix. This matrix establishes a connection between actual and reactive power and the minor variations in voltage magnitude and phase angle.

$$\begin{bmatrix} \Delta P \\ \Delta Q \end{bmatrix} = \begin{bmatrix} J_1 & J_2 \\ J_3 & J_4 \end{bmatrix} \begin{bmatrix} \Delta\delta \\ \Delta |V| \end{bmatrix} \tag{7}$$

In 8 and 9, the power residual is described in terms of the Jacobian matrices $J_1$, $J_2$, $J_3$, and $J_4$ that are integral to the Newton-Rapson method.

$$\Delta P_i^k = P_i^{sch} - P_i^k \tag{8}$$

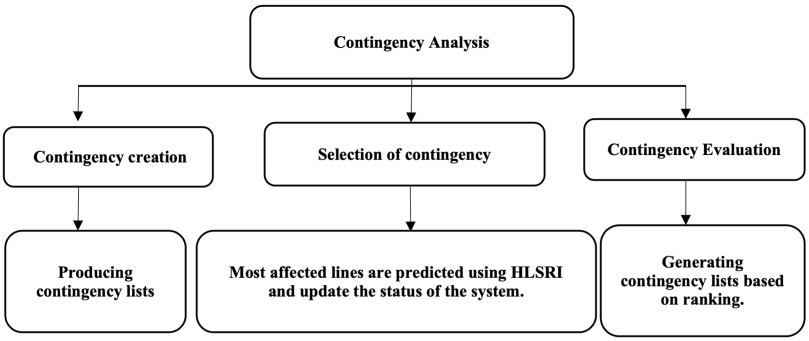


**Figure 1: Classification of Contingencies**

$$\Delta Q_i^k = Q_i^{sch} - Q_i^k \tag{9}$$

The new estimates for the voltage's angle and magnitude are represented in equation 10 and equation 11.

$$\delta_i^{k+1} = \delta_i^k - \Delta\delta_i^k \tag{10}$$

$$\left|V_i^{k+1}\right| = \left|V_i^k\right| - \left|\Delta V_i^k\right| \tag{11}$$

These two load models analyze load behavior in IEEE-30 Bus systems. rating index helps locate severe lines.

## 3 Power System Contingency Ranking Approach

Contingency analysis is a standard practice in contemporary Energy Management Systems, where power grid planning can be subject to variations based on the outcomes of system contingency analysis. The interruption of a single line has the potential to overload adjacent branches and induce swift changes in the voltage profile. The assessment of power system security involves assigning severity rankings. The investigation is streamlined, as depicted in Figure 1.

### 3.1 A New Proposed Ranking Index

The proposed measure, referred to as HLSRI, is derived from the line and fast voltage stability indexes. In equation 12, it is depicted as HLSRI, as illustrated in [3].

$$\begin{aligned} HLSRI &= \tfrac{4XQ_n}{[V_m]^2}\left[\tfrac{|Z|^2}{X_{Line}}\beta - \tfrac{XQ_n}{[\sin(\theta-\delta)]^2}(\beta-1)\right] \leq 1, \\ \text{where } \beta &= \left\{ \begin{array}{ll} 1 & \delta < \delta_C \\ 0 & \delta \geq \delta_C \end{array} \right\}, \end{aligned} \tag{12}$$

where $\delta$ is a modifier and $\beta$ is a toggling function.

The stability of the system is compromised when the HLSRI value approaches 1; conversely, it is considered safe and stable under other circumstances. The introduced index has been implemented on the IEEE 30 bus system utilizing the Newton-Raphson method. The test system comprises six generators, 24 load buses, and 41 transmission lines, and it is derived from historical data provided by IEEE.

### 3.2 Artificial Neural Networks

Various factors contribute to the variability of power systems. Traditional offline methods were unable to provide continuous monitoring of system security. Enhancing security monitoring and online implementation involves training an ANN to handle unforeseen requirements. This approach aims to predict the size of emergency systems and employs active power and voltage performance indicators to rank potential outcomes, facilitating a quick and accurate assessment of security. The evaluation of system operation and the ranking of severity are integral components of this process. The block diagram in Figure 2 illustrates the structure of the ranking module. Module inputs include active and reactive power, voltage magnitudes (V), and N-1 line outage contingencies. These inputs encompass all operational conditions ($K_i$). The module utilizes the Radial Basis Function Network (RBFN) method, where nodes estimate performance. Figure 3 provides an example of an ANN-RBFN model employed for forecasting performance indices. This model considers alternative outcomes to forecast operational security posture performance indicators.

The Radial Basis Function Network method is employed to train the IEEE test system in predicting the HLSRI and security within the realm of ANN. The values generated by the proposed index in ANN closely approximate those obtained through the NR method. The values produced by the proposed index are being considered. The processing of the proposed index is carried out using machine learning techniques.

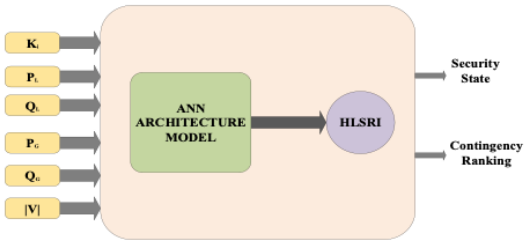


**Figure 2: Block diagram of Ranking Module**

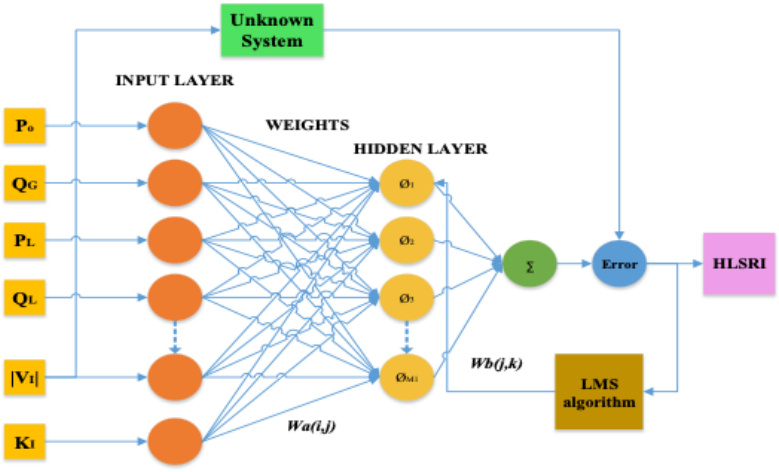


**Figure 3: RBFN Model for the prediction of performance indices**

## 4 Methodology

### 4.1 Machine Learning

Contingency analysis stands as a widely employed practice in modern energy management systems, wherein the outcomes of this analysis can significantly impact the power grid planning process. The potential repercussions of a disruption in a solitary power line are extensive, as it may lead to undue burdens on neighboring branches, thereby causing sudden fluctuations in voltage profiles. The assessment of the power system's security is carried out through a contingency ranking rooted in severity. The three fundamental steps involved in streamlining the analysis process are depicted in Figure 1 [4] [5].

Figure 3 illustrates the classification of J48. The diagram in Figure 4 is conclusive. A single branch extends from the 5-foot tree, featuring three leaves. The HLSRI range fluctuates, while decision tree size and leaf count remain consistent. The ranking is determined by three states of the test system.

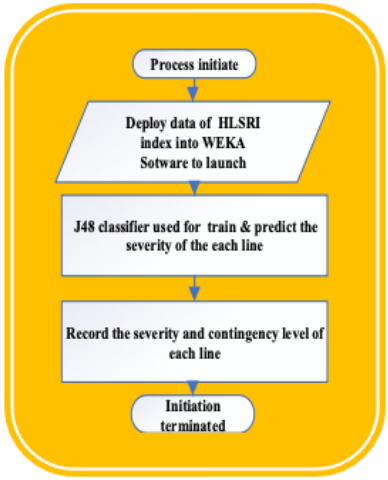


**Figure 4: Data processing and Classification of Transmission Line Severity**

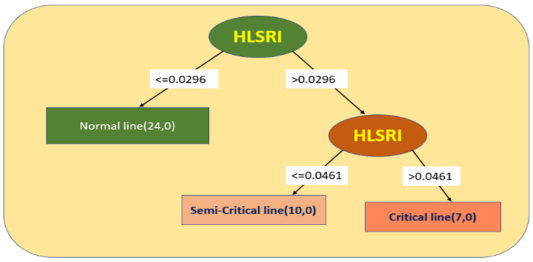


**Figure 5: J48 Classifier tree Visualizer with HLSRI for IEEE 30 Bus**

**Table 1: Confession matrix of IEEE30 bus system**

| Classifier Type | Training (70%) | Testing (30%) |
|---|---|---|
| Machine Learning -HLSRI | $\begin{matrix} & \Pr edicted & \\ Actual & \begin{bmatrix} 1 & 0 & 0 \\ 0 & 6 & 0 \\ 0 & 0 & 5 \end{bmatrix} \end{matrix}$ | $\begin{matrix} & \Pr edicted & \\ Actual & \begin{bmatrix} 0 & 2 & 0 \\ 0 & 12 & 0 \\ 0 & 1 & 14 \end{bmatrix} \end{matrix}$ |
| ANN-RBFN | $\begin{matrix} & \Pr edicted & \\ Actual & \begin{bmatrix} 2 & 0 & 0 \\ 0 & 8 & 0 \\ 0 & 0 & 3 \end{bmatrix} \end{matrix}$ | $\begin{matrix} & \Pr edicted & \\ Actual & \begin{bmatrix} 0 & 3 & 0 \\ 0 & 13 & 0 \\ 0 & 1 & 11 \end{bmatrix} \end{matrix}$ |

**===J8-Classifier model ====**
**J48 tree Structure for IEEE 30**

1) Stresse line or Critical (7.0) : HLSRIIEEE30$>$ 0.0461
2) Semi-Stresse line (10.0) : 0.0296 $>$HLSRI IEEE30$\leq$ 0.0461
3) Normal line (24.0) : HLSRI IEEE30$<$ 0.0296

Visualize by Weka-J48

In Machine learning and ANN-RBFN methods, 70 % of data is trained and % of data is tested and a comparative graph of line no. Vs HLSRI for ML- HLSRI and ANN-RBF of IEEE 30 Bus system as shown in Figure 5 and Confession Matrices for IEEE-30 as shown in Table 1.

The computational time of the test system by using the Machine learning- J48 algorithm is 0.006 sec when compared to RBFN.

## 5 Designing Custom Power Devices Mathematically

FACTS appliance control limitations are predicted via injection models (Basu 2008). Interline power flow controller (IPFC) and Unified power flow controller (UPFC) assist test system power flows and stability during contingencies better than other FACTS devices. UPFC and IPFC's mathematical modeling is summarized here. [6]–[8]

### 5.1 Shunt and Series Controller

There are two controllers at work in a unified power flow system. Which is linked to the transmission line through DC link capacitors shared by the shunt and series VSCs. The series compensator (SSSC) is a term used in a 2007 study by Vural et al. The arrangement converter's yield voltage is added to the nodal voltage at bus i to get the final nodal voltage at bus j. How the power's intensity is controlled is shown by the $\delta_{CR}$ phase angle, and The yield voltage specifies the voltage's direction. $V_{cR}$] A three-stage UPFC is supported by two voltage sources and power restrictions.

$$E_{VR} = V_{CR}(Cos\delta_{CR} + jSin\delta_{CR}) \tag{13}$$

$$R_e = \{-E_{VR}I_{VR} + E_{VR}I_m\} \tag{14}$$

Active and reactive power equations are as follows at bus i.

$$P_i = \{V_i^2 G_{ii} + V_i V_j[G_{ij}Cos(\theta_i - \delta_j) \ + B_{ij}Sin(\theta_i - \delta_j)] + \ V_i V_{CR}[G_{ij}Cos(\theta_i - \delta_{CR}) + B_{ij}Sin(\theta_i - \delta_{CR})] + V_i V_{CR}[G_{VR}Cos(\theta_i - \delta_{CR}) + B_{ij}Sin(\theta_i - \delta_{CR})]\}\left[P_1 V_i^2 + P_2 V_i + P_3\right] \tag{15}$$

$$Q_i = \{-V_i^2 B_{ii} + V_i V_j[G_{ij}Sin(\theta_i - \delta_j) \ - B_{ij}Cos(\theta_i - \delta_j)] + V_i V_{CR}[G_{ij}Sin(\theta_i - \delta_{CR}) - B_{ij}Sin(\theta_i - \delta_{CR})] + V_i V_{CR}[G_{VR}Sin(\theta_i - \delta_{CR}) - B_{ij}Cos(\theta_i - \delta_{CR})]\}\left[P_1 V_i^2 + P_2 V_i + P_3\right] \tag{16}$$

where $G_{ij}$ and $B_{ij}$ are the conductance and susceptance between bus i and bus j, respectively. The above Equation 15 and 16 modified UPFC with ZIP load model.

### 5.2 Interline Power Flow Controller

The IPFC typically makes use of many DC-to-AC converters, all of which provide series compensation for a different line. The IPFC includes several static synchronous series compensators (SSSC). All of the converters have high reactive power transmission and storage capacities (Zhang et al. 2006b). A series converter connected between bus i and bus j can provide complicated power, as described by Equations 17, 17, 18, 19, and 20 in that order [9].

$$P_{ij} = \{V_i^2 G_{ii} - \sum_{\substack{j=1 \\ j \neq i}}^{n} V_i V_{ij}(G_{ij} Cos\theta_{ij} - B_{ij} Sin\theta_{ij}) + \sum_{\substack{j=1 \\ j \neq i}}^{n} V_i V_{seij}(G_{ij} Cos(\theta_{ij} - \theta_{seij}) - B_{ij} Sin(\theta_{ij} - \theta_{seij}))\} \left[P_1 V_i^2 + P_2 V_i + P_3\right] \tag{17}$$

$$Q_{ij} = \{V_i^2 B_{ii} - \sum_{\substack{j=1 \\ j \neq i}}^{n} V_i V_{ij}(G_{ij} Sin\theta_{ij} - B_{ij} Cos\theta_{ij}) - \sum_{\substack{j=1 \\ j \neq i}}^{n} V_i V_{seij}(G_{ij} Sin(\theta_{ij} - \theta_{seij}) - B_{ij} Cos(\theta_{ij} - \theta_{seij}))\} \left[P_1 V_i^2 + P_2 V_i + P_3\right] \tag{18}$$

$$P_{ji} = \{V_i^2 G_{ii} - \sum_{\substack{j=1 \\ j \neq i}}^{n} V_i V_{ji}(G_{ij} Cos\theta_{ji} - B_{ij} Sin\theta_{ji}) - \sum_{\substack{j=1 \\ j \neq i}}^{n} V_i V_{se_{ij}}(G_{ij} Cos(\theta_{ij} - \theta_{seij}) - B_{ij} Sin(\theta_{ij} - \theta_{seij}))\} \left[P_1 V_i^2 + P_2 V_i + P_3\right] \tag{19}$$

$$Q_{ji} = \{V_i^2 B_{ii} - \sum_{\substack{j=1 \\ j \neq i}}^{n} V_i V_{ji}(G_{ij} Cos\theta_{ji} - B_{ij} Sin\theta_{ji}) - \sum_{\substack{j=1 \\ j \neq i}}^{n} V_i V_{se_{ij}}(G_{ij} Sin(\theta_{ij} - \theta_{se_{ij}}) - B_{ij} Cos(\theta_{ij} - \theta_{se_{ij}}))\} \left[P_1 V_i^2 + P_2 V_i + P_3\right] \tag{20}$$

where $V_i$ and $V_j$ stand for the maximum allowed bus i and j voltages (p.u.), and $V_{seijk}$ and the conjugate of $I_{ijk}$ stand for the maximum allowed bus i, j, and k series voltage and the reference current. Mathematical expressions of IPFC incorporated in ZIP load model to assess its behavior and the above Equations 17, 17, 18, 19, and 20 modified IPFC mathematical expression with ZIP load model.

## 6 Objective Function

The novel approach lowers the consumption of fuel by using the objective function and stress on the transmission line. Optimal fuel and compensation device costs must be considered together to arrive at a workable solution. The desired function is shown here in Equation 21.

$$objective\ function(F) = \min(F_1 + F_2 + F_3) \tag{21}$$

A set of individual iterations for an objective function (F) are designated by the respective numbers F1, F2, and F3 in this case. The main aim of the objective function is to reduce the fuel cost and cost of the compensation devices and effective utilization of generator capacity.

### 6.1 Optimization of Real Power Loss

The amount of active power being lost has been reduced to an absolute minimum at this stage. Reducing real power loss in transmission lines is demonstrated by Equation 21, which illustrates the preliminary objective function effectively.

$$F_1 = P_{Loss} = \sum_{k=1, J \neq i}^{n} G_{kj}[V_k^2 + V_j^2 - 2V_k V_j Cos(\delta_k - \delta_j) \tag{22}$$

where $P_{Loss}$ is power loss, $N_{Line}$ is transmission lines, $G_{kj}$ is conductance at bus k and j's, $V_k$ and $V_j$ are voltages and$\delta_k \delta_j$, angles.

### 6.2 Investments in FACTS Equipment

Here, the investment expressed in $/h for UPFC and IPFC is analyzed using Equation 23.

$$F_2 = Cost_{UPFC} + Cost_{IPFC} \tag{23}$$

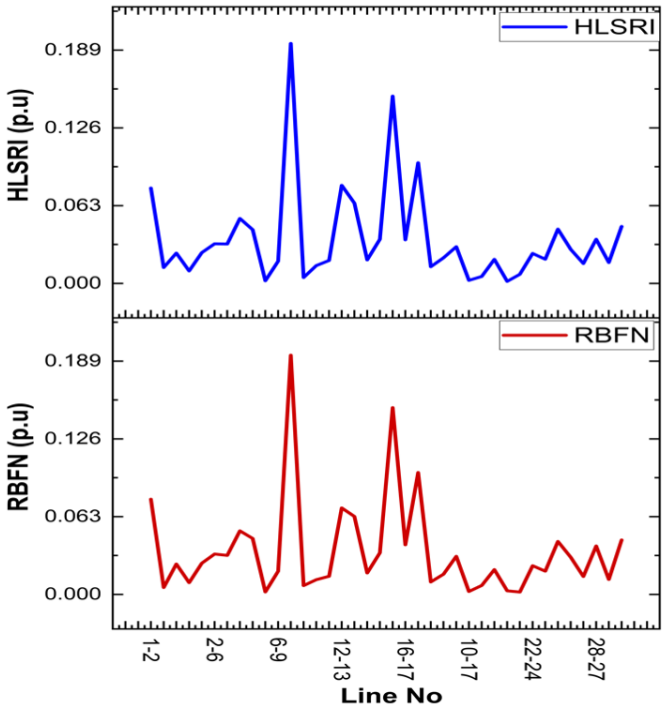


**Figure 6: A Comparative graph of line no. Vs HLSRI for ML- HLSRI and ANN-RBF of IEEE 30 Bus system**

**Table 2: Confession matrix of IEEE30 bus system**

| Overloading | Total Generation Capacity (MW) | Total Active Power Loss (MW) | Fuel Cost($/hrs) | Total Generation Capacity (MW) |
|---|---|---|---|---|
| 1 | 17.04 | 312.23 | 283.4 | 614.48 |
| 1.3 | 36.16 | 439.29 | 368.42 | 868.61 |
| 1.5 | 53.70 | 527.91 | 425.1 | 1045.85 |

where

$$Cost_{UPFC} = 0.0003s^2 - 0.026911s + 188.22$$
$$Cost_{IPFC} = Cost_{IPFCA} + Cost_{IPFCB}$$
$$Cost_{IPFCA} = 0.00015s_i^2 - 0.0134s_i + 94.11$$
$$Cost_{IPFCB} = 0.00015s_j^2 - 0.0134s_j + 94.11$$

$$s = |Q_2| - |Q_1|\,;\quad s_i = |Q_{i2}| - |Q_{i1}|\,;\ s_j = |Q_{i2}| - |Q_{i1}|$$

After MVAR line compensation has been established, the reactive power flow (Q2) will be higher than the reactive power flow (Q1) in the line. The reactive power flow down the line is represented by Qi1 and Qi2, and the cost function Sij of the converters linked to buses i and j.

### 6.3 Cost Reduction of Fuel

Reduced fuel costs in the generator have finally been realized. The cost of fuel for the generator can be thought of as the quadratic of the sum of the costs involved in using fuel functions that are themselves convex (Lagrange Iteration Method(LIM)). Equation 24 depicts the generators' quadratic fuel cost function.

$$F_3 = Min\cos t_f(x)\sum_{i=1}^{N_g}[a_i p_{gi}^2 + b_i p_{gi} + c_i p_{gi}] \tag{24}$$

Ng is the total number of generators; The bus index is I, the ith generator's fuel cost coefficients are bi and ci, and its maximum active power output is Pgi.

## 7 Results and Discussion

### 7.1 Case-1: Machine Learning Algorithm Applied For the Test System

Location of the FACTS device using ML and fuel cost calculated with the exiting generator capacity and it is tabulated below. In this study, we analyze the IEEE 30 bus system using the ZIP load model and demonstrate its behavior under varying loads and interruptions to the power supply.

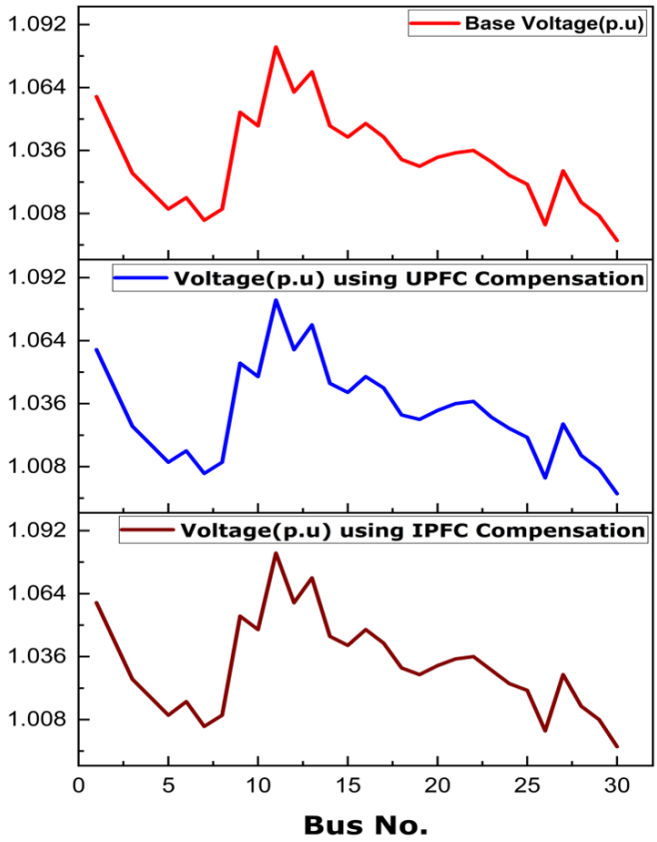


**Figure 7: Bus No. vs voltage for IEEE-30 Bus**

**Table 3: Power transfer Capability of FACTS devices**

| Conditions | | Custom power devices-UPFC | | | Custom power devices-IPFC | | |
|---|---|---|---|---|---|---|---|
| | | Location | Base case | P(MW) | Location | Base case | P(MW) |
| Line outage | 2-4 | 6-10 | 15.286 | 23.425 | 6-10-28 | 15.2861 | 18.104 |
| | 3-4 | 14-15 | 1.611 | 11.069 | 14-15-23 | 1.611 | 1.957 |
| | 2-5 | 15-18 | 5.9258 | 11.452 | 15-18-23 | 5.9258 | 7.758 |
| Overloading | 1 | 6-10 | 15.286 | 23.425 | 6-10-28 | 15.286 | 18.104 |
| | 1.3 | 15-18 | 8.342 | 13.559 | 15-18-23 | 8.3423 | 9.702 |
| | 1.5 | 15-18 | 9.990 | 12.879 | 15-18-23 | 9.990 | 10.777 |

Table 2 shows the base case results of the IEEE 30 bus system and Table 3 shows the power transfer enhancement using custom power devices. The below Table 4 shows the fuel cost with generation capacity during line outage conditions and overloading conditions.

From Table 4, it is clear that the optimum location of FACTS device-based HLSRI is generated from the J48 algorithm of the machine learning tool. The minimum fuel cost was achieved with the help of objective functions, and it fulfills the requirement. i.e., minimization of loss and enhancement of power transfer capability with minimum fuel cost.

### 7.2 Case-2: Machine Learning Algorithm With PSO Applied For The Test System

In Case 1, a standard IEEE 30 bus system was analyzed, and out of its six generators, only two were used to meet the system's overall demand. As a result, losses have risen.

**Table 4: Power Losses and Fuel costs of FACTS devices**

| Conditions | | Custom | Power | Devices | -UPFC | Custom | Power | Devices | -IPFC |
|---|---|---|---|---|---|---|---|---|---|
| | | Location | Total Ploss (MW) | Total Generation Capacity (MW) | Fuel Cost($/hr) | Location | Total Ploss (MW) | Total Generation capacity (MW) | Fuel Cost($/hr) |
| Outage | 2-4 | 6-10 | 16.46 | 290.67 | 571.36 | 6-10-28 | 15.90 | 290.7 | 571.42 |
| | 3-4 | 14-15 | 16.40 | 288.55 | 567.12 | 14-15-23 | 16.15 | 290.4 | 570.83 |
| | 2-5 | 15-18 | 15.91 | 285.69 | 561.40 | 15-18-23 | 15.84 | 292.33 | 574.69 |
| Over-loading | 1 | 6-10 | 16.46 | 290.67 | 571.36 | 6-10-28 | 15.90 | 290.70 | 57.421 |
| | 1.3 | 15-18 | 30.83 | 386.53 | 763.08 | 15-18-23 | 30.62 | 384.8 | 759.62 |
| | 1.5 | 15-18 | 45.29 | 462.79 | 915.60 | 15-18-23 | 43.94 | 455.65 | 901.32 |

**Table 5: Cost of the custom power devices**

| Condition | Location | UPFC Cost ($/h) | IPFC Cost ($/h) |
|---|---|---|---|
| Line outage | 6-10 | 187.58 | 188.12 |
| | 14-15 | 188.17 | 188.15 |
| | 15-18 | 188.01 | 188.09 |
| Overloading | 6-10 | 187.58 | 188.12 |
| | 15-18 | 187.75 | 188.10 |
| | 15-18 | 188.07 | 188.11 |

**Table 6: Base case Results for different Loadings**

| Conditions | | Total Generation | Capacity (MW) | Total Active Power | Loss (MW) | Fuel Cost | ($/hr) |
|---|---|---|---|---|---|---|---|
| | | ML | ML+PSO | ML | ML+PSO | ML | ML+PSO |
| Overloading | 1 | 312.230 | 298.0564 | 17.0411 | 6.8581 | 614.483 | 576.9212 |
| | 1.3 | 439.297 | 403.3304 | 36.161 | 16.8133 | 868.6166 | 787.4691 |
| | 1.5 | 527.917 | 491.1514 | 53.7077 | 29.7025 | 1045.856 | 963.1111 |

In the case-2 location of the FACTS, the device was identified with ML, and fuel cost was calculated with optimum utilization of generator capacity using the Particle Swarm Optimization (PSO) algorithm for the modified IEEE30 bus system, and it is tabulated below [10].

Table 6 shows a comparative analysis of the Machine learning algorithm and Machine learning algorithm with PSO for optimum utilization of generator capacity. The total generation capacity, Loss, and fuel cost tabulated.

Table 7 shows the power flow enhancement during contingency and overloading conditions with compensation.

Tables 8 and 9 show the optimal generation capacity utilization with minimum fuel cost by using ML along with PSO for UPFC and IPFC compensation, and it is clear that the minimum fuel cost achieved by using ML for objective functions fulfills the requirement.

## 8 Conclusions

In this paper, the integration of various renewable and nonrenewable energy sources into the grid by utilities to meet escalating demand is challenged by issues in generators, transmission lines, and distribution networks, particularly during sudden load changes has been investigated with mathematical modelling and analysis. The success of predicting future load behavior lies in the crucial role of load representation, with ZIP load models incorporating contingency criteria proving effective. ANNs are trained to forecast line losses and system reactions, while the HLSRI is employed in nonlinear techniques for contingency ranking. The study underscores the significance of power outages and load fluctuations, emphasizing the critical role they play in determining the power grid's status.

## Acknowledgment

The authors like to acknowledge the Department of Electrical and Electronics Engineering, Sree Vidyanikethan Engineering College, Andhra Pradesh, India and Jawaharlal Nehru Technological University, Anantapur, Andhra Pradesh, India for providing the research facilities to conduct this joint research work.

**Table 7: Power Losses and Fuel Costs of UPFC devices**

| Conditions | | Custom | Power | Devices-UPFC | Custom | Power | Devices-IPFC |
|---|---|---|---|---|---|---|---|
| | | Location | ML- P(MW)-base case | ML+PSO P (MW) | Location | ML- P(MW)-base case | ML+PSO P(MW) |
| Line outage | | 6-10 | 12.408 | 17.150 | 6-10-28 | 12.408 | 12.280 |
| | | 14-15 | 1.943 | 6.712 | 14-15-23 | 1.943 | 2.566 |
| | | 15-18 | 6.597 | 8.273 | 15-18-23 | 6.597 | 11.556 |
| Over-loading | 1 | 6-10 | 12.408 | 17.150 | 6-10-28 | 12.408 | 12.280 |
| | 1.3 | 15-18 | 8.824 | 10.140 | 15-18-23 | 8.824 | 13.304 |
| | 1.5 | 15-18 | 10.651 | 11.378 | 15-18-23 | 10.651 | 19.021 |

**Table 8: Power Losses and Fuel Costs of UPFC devices**

| | Custom | Power | Devices | -UPFC | Compensation | |
|---|---|---|---|---|---|---|
| Conditions | Total Active | power Loss (MW) | Total Generation | capacity (MW) | Fuel Cost | ($/hr) |
| Algorithms | ML | ML+PSO | ML | ML+PSO | ML | ML+PSO |
| Line outage | 16.464 | 6.659 | 290.674 | 285.370 | 571.369 | 551.549 |
| | 16.406 | 6.781 | 288.553 | 285.553 | 567.127 | 551.916 |
| | 15.919 | 6.773 | 285.691 | 286.439 | 561.403 | 553.688 |
| Overloading | 16.464 | 6.659 | 290.674 | 285.370 | 571.369 | 551.549 |
| | 30.838 | 15.827 | 386.534 | 380.847 | 763.089 | 742.502 |
| | 45.293 | 25.154 | 462.794 | 447.206 | 915.609 | 875.222 |

**Table 9: Power Losses and Fuel Costs of UPFC devices**

| | Custom | power | devices | -IPFC | Compensation | |
|---|---|---|---|---|---|---|
| Conditions | Total | Generation | capacity | (MW) | Fuel | Cost($/hr) |
| Algorithms | ML | ML+PSO | ML | ML+PSO | ML | ML+PSO |
| Line outage | 15.907 | 6.601 | 283.952 | 284.233 | 571.421 | 549.276 |
| | 16.151 | 6.69 | 287.724 | 284.797 | 570.833 | 550.403 |
| | 15.849 | 6.76 | 284.110 | 284.466 | 574.697 | 549.740 |
| Overloading | 15.907 | 6.601 | 283.952 | 284.233 | 571.421 | 549.276 |
| | 30.628 | 15.813 | 384.8 | 378.773 | 759.621 | 738.355 |
| | 43.949 | 24.099 | 455.65 | 437.397 | 901.321 | 855.602 |

## Competing Interests

The authors declare that they have no competing interests.

## Authors Contributions

The authors confirm contribution to the paper as follows: study conception and design: PV, NV, data collection: PV, NV; analysis and interpretation of results: PV, NV; draft manuscript preparation: PV. All authors reviewed the results and approved the final version of the manuscript.

## References

[1] L. Ma, L. Wang, and Z. Liu, ''Soft open points-assisted resilience enhancement of power distribution networks against cyber risks,'' *IEEE Transactions on Power Systems*, vol. 38, no. 1, pp. 31–41, 2023.

[2] Z. Chu, S. Lakshminarayana, B. Chaudhuri, and F. Teng, ''Mitigating load-altering attacks against power grids using cyber-resilient economic dispatch,'' *IEEE Transactions on Smart Grid*, vol. 14, no. 4, pp. 3164–3175, 2023.

[3] P. Venkatesh and N. Visali, ''Machine learning for hybrid line stability ranking index in polynomial load modeling under contingency conditions,'' *Intelligent Automation  Soft Computing*, vol. 37, no. 1, pp. 1001–1012, 2023.

[4] M. M. Roomi, W. S. Ong, S. M. S. Hussain, and D. Mashima, ''Iec 61850 compatible openplc for cyber attack case studies on smart substation systems,'' *IEEE Access*, vol. 10, pp. 9164–9173, 2022.

[5] S. Wang, Y. Jin, and M. Cai, ''Enhancing the robustness of networks against multiple damage models using a multifactorial evolutionary algorithm,'' *IEEE Transactions on Systems, Man, and Cybernetics: Systems*, vol. 53, no. 7, pp. 4176–4188, 2023.

[6] P. Venkatesh and N. Visali, ''Application of machine learning to generate a contingency ranking for power system security,'' in *2023 Third International Conference on Artificial Intelligence and Smart Energy (ICAIS)*, I. Coimbatore, Ed., 2023, pp. 590–595.

[7] A. A. Eladl, M. I. Basha, and A. A. ElDesouky, ''Multi-objective-based reactive power planning and voltage stability enhancement using facts and capacitor banks,'' *Electrical Engineering*, vol. 104, no. 5, pp. 3173–3196, 2022.

[8] X. Chen, L. Huang, D. Zheng, J. Chen, and X. Li, ''Research and application of communication security in security and stability control system of power grid,'' in *2022 Seventh Asia Conference on Power and Electrical Engineering (ACPEE)*, C. Hangzhou, Ed., 2022, pp. 1215–1221.

[9] B. L. al., ''The voltage security region calculation method of receiving-end power system based on the equivalence of transient process,'' *IEEE Access*, vol. 10, pp. 95 083–95 092, 2022.

[10] H. Delkhosh and H. Seifi, ''Power system frequency security index considering all aspects of frequency profile,'' *IEEE Transactions on Power Systems*, vol. 36, no. 2, pp. 1656–1659, 2021.